SUPPORTING INFORMATION

Polymethylated Aromatics Deactivate Intracrystalline Acid Sites in MFI Zeolites during Low-Temperature Toluene Methylation

Sopuruchukwu Ezenwa, Andrew T. Norfleet, David Hibbitts, Rajamani Gounder*

Davidson School of Chemical Engineering, Purdue University, West Lafayette, IN, 47907, USA

*Corresponding author. E-mail: rgounder@purdue.edu

Table of Contents

Section S1. Influence of reactor-bed residence times on toluene methylation in MFI

For MFI-TPA-C and MFI-EDA-1, measured toluene methylation rates and xylene isomer selectivity as a function of time-on-stream are shown for varying packed-bed reactor residence times (quantified here as reactant site-contact times) (Figures S1 and S2). The site-contact times are varied (1.5–14.5 s mol H^+ (mol toluene)$^{-1}$) by changing the loading of the MFI sample (of fixed H^+ density) in the reactor bed or the total gas flow rates at fixed reactant pressures (4 kPa toluene, 66 kPa DME). Our previous report [1] showed that initial aromatic formation rates and xylene isomer selectivity in MFI zeolites are almost independent of the site-contact times and the toluene conversions increased linearly with site-contact times, demonstrating differential reactor operation during toluene methylation on aluminosilicates at low temperatures (403 K) and conversions (<1%). On MFI-TPA-C and MFI-EDA-1, the curves of the toluene methylation rates and xylene isomer selectivity versus time on stream are almost overlaid on top of each other within the range of site-contact times tested (Fig. S1a–b, Fig. S2a–b), albeit with slight variations that are non-systematic and within the range of experimental uncertainties.

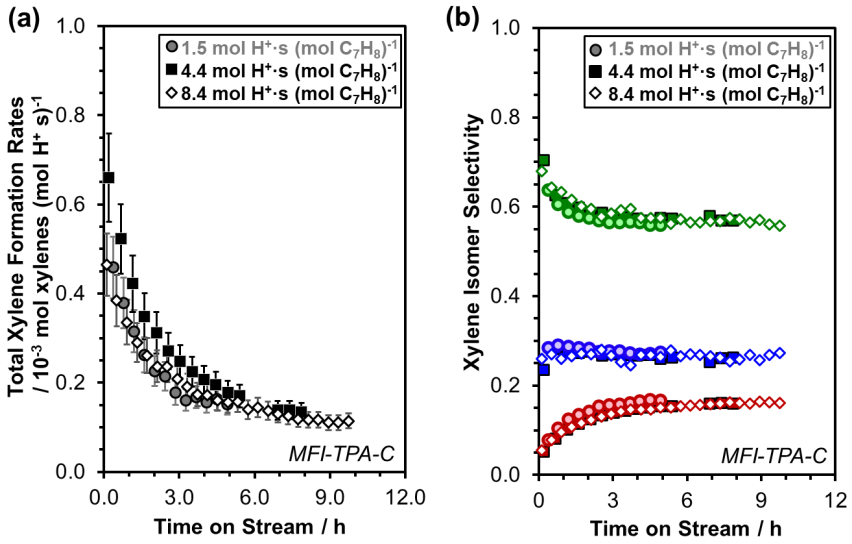

Figure S1. (a) Total xylenes formation rates and (b) xylene isomer selectivity as a function of time on stream on MFI-TPA-C during toluene methylation (4.0–4.4 kPa toluene, 66 kPa DME, 403 K) and varying reactor bed residence times (1.5, 4.4 and 8.4 s mol H^+ (mol toluene)$^{-1}$). Uncertainties in rate measurements are ±15%.

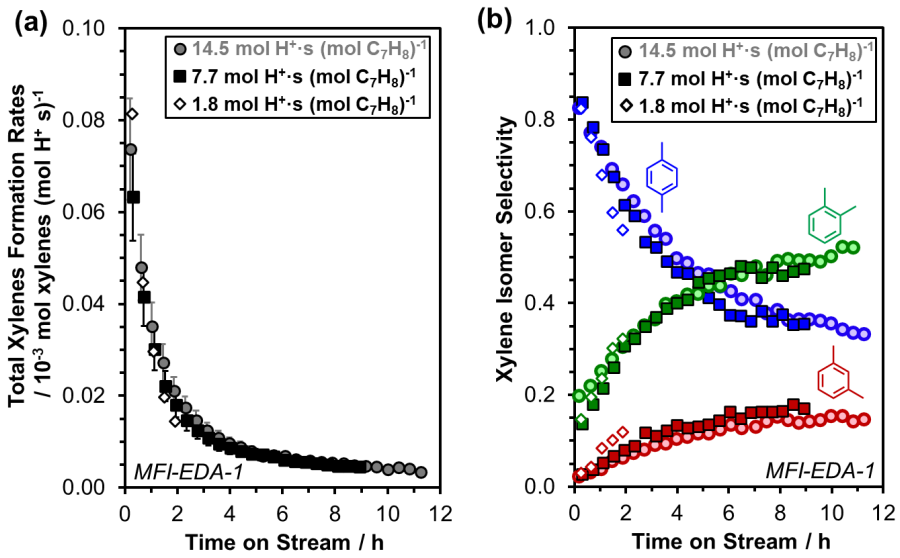

Figure S2. (a) Total xylenes formation rates and (b) xylene isomer selectivity as a function of time on stream on MFI-EDA-1 during toluene methylation (4.0–4.1 kPa toluene, 66 kPa DME, 403 K) and varying reactor bed residence times (1.8, 7.7 and 14.5 s mol H^+ (mol toluene)$^{-1}$). Uncertainties in rate measurements are ±15%.

The overlaid xylene formation rates and isomer selectivity profiles with times on stream for varying initial site contact times (Fig. S1a–b, Fig. S2a–b) suggest that changes in the reactivity and selectivity with time on stream do not solely reflect changes in the effective site-contact times due to decreases in total number of H^+ sites. If so, the initial selectivities could have depended on the initial site contact times. Rather, as discussed in the main text (Section 3.2), the nature of deactivation during low-temperature toluene methylation is selective on MFI zeolites, because of changes to both the number and the relative proportions of distinct H^+ site ensembles (i.e., intracrystalline H^+ and extracrystalline H^+ sites).

To obtain a further insight into the nature of deactivation, the temporal xylenes formation rates for MFI-TPA-C and MFI-EDA-1 are plotted against the estimated toluene conversion to gas-phase aromatic product on the deactivating catalyst (Figs. S3 and S4). For the different initial site-contact times, the initial toluene methylation rates (per initial total H^+) and xylene isomer selectivities (i.e., when extrapolated to zero times on stream [1]) are invariant of initial site contact times (or initial conversions). As the conversions decreased with deactivation (i.e., from right to left of Fig. S3a and Fig. S4a), the toluene methylation rates (per initial total H^+) for different initial site contact times asymptotically approached the same values (i.e., zero formation rates at zero toluene conversion). The almost linear dependence of the temporal total aromatic formation rates

on the deactivation-induced conversion changes is partly a consequence of the functional form of the equations used to calculate toluene methylation rates and toluene conversion at these low conversions (i.e., based on moles of aromatic products formed rather than toluene consumed; Equation 2 and Equation 4 in main text) and partly a consequence of decreases in the accessibility of the site ensembles with the most abundant fraction and highest reactivities (i.e., intracrystalline H^+). Furthermore, the decreasing toluene methylation rates (per initial total H^+) at iso-conversion with increasing initial-site contact times (i.e., a vertical slice of the data in Fig. S3a and Fig. S4a), reflects the varying proportions of accessible H^+ sites which are much lower on a mostly deactivated catalyst bed (e.g., at 0.02% toluene conversion for 14.5 s mol H^+ (mol toluene)$^{-1}$ on MFI-EDA-1) than a fresh catalyst bed (e.g., at 0.02% toluene conversion for 1.8 s mol H^+ (mol toluene)$^{-1}$ on MFI-EDA-1).

On the other hand, for different initial site-contact times on either MFI-TPA-C and MFI-EDA-1, the initial xylene isomer selectivities (i.e., when extrapolated to zero times on stream [1]) are independent of initial site contact times or initial conversions (Fig. 3b–c and Fig. S4b–c). As the conversions decreased with deactivation (i.e., from right to left of Fig. 3b–c and Fig. S4b–c), the xylene isomer selectivities for different initial site contact times asymptotically approached the same values (i.e., non-zero constant values at zero toluene conversion). As a consequence, the curves of the xylene isomer selectivity versus conversion as a result of deactivation for either MFI-TPA-C (Fig. S3b–c) or MFI-EDA-1 (Fig. S4b–c) at varying contact times are not overlaid indicating that the temporal changes in selectivity during catalyst deactivation are not solely because of decreases in effective site-contact times arising from loss of active sites of equal reactivity and selectivity. At iso-conversion on fresh and deactivated MFI catalysts (from different initial site contact times), the xylene isomer selectivities differ significantly (Fig. 3b–c and Fig. S4b–c). Rather, based on discussion in Section 3.2. in main text, changes in selectivity with time on stream reflect changes in both the total numbers and proportions of distinct site ensembles having unique reactivity and selectivity behavior during toluene methylation. Together, these results demonstrate that the nature of deactivation during low-temperature toluene methylation in MFI is selective [2–5].

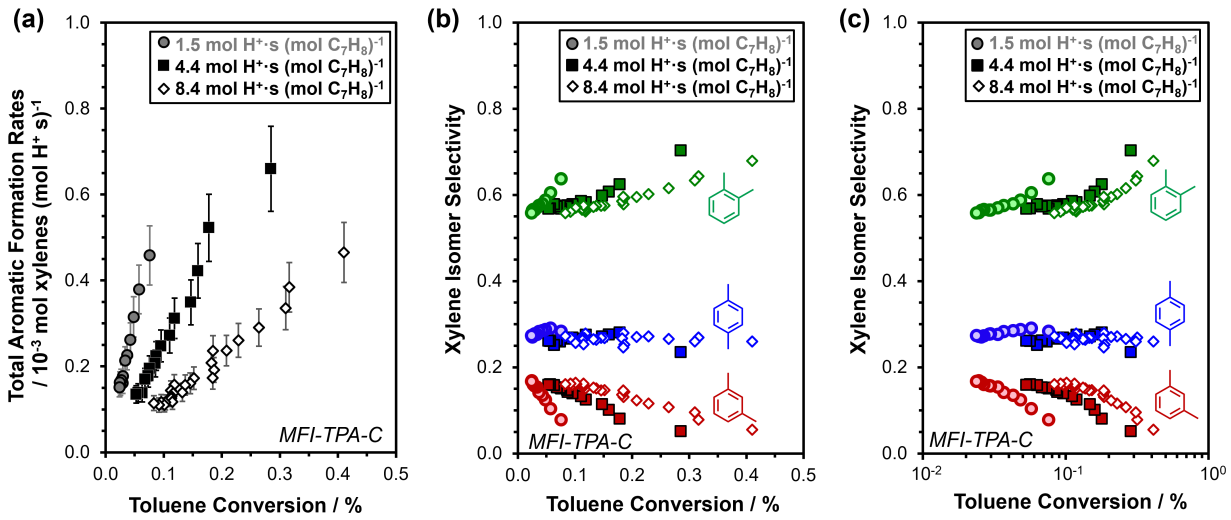

Figure S3. (a) Total xylenes formation rates and (b) xylene isomer selectivity as a function of conversion as a result of deactivation during toluene methylation (4.0–4.4 kPa toluene, 66 kPa DME, 403 K) on MFI-TPA-C at varying reactor bed residence times (1.5, 4.4 and 8.4 s mol H^+ (mol toluene)$^{-1}$). For clarity, the xylene isomer selectivity as a function of conversion as a result of deactivation are presented in a linear-log plot in (c).Uncertainties in rate measurements are ±15%.

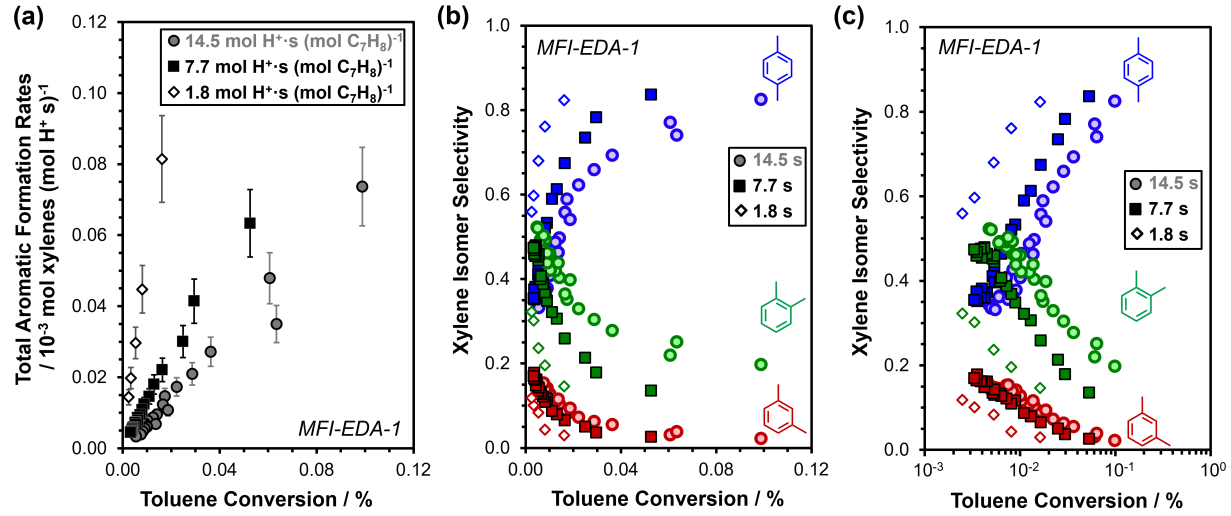

Figure S4. (a) Total xylenes formation rates and (b) xylene isomer selectivity as a function of conversion as a result of deactivation during toluene methylation (4.0–4.1 kPa toluene, 66 kPa DME, 403 K) on MFI-EDA-1 at varying reactor bed residence times (1.8, 7.7 and 14.5 s mol H^+ (mol toluene)$^{-1}$). For clarity, the xylene isomer selectivity as a function of conversion as a result of deactivation are presented in a linear-log plot in (c). Uncertainties in rate measurements are ±15%.

Section S2. Additional discussion on molecular dimensions of C_6–C_{12} methylbenzenes

Earlier studies have established that measured [6–10] or calculated [11] intracrystalline diffusivities (or diffusional barriers) of commonly studied $C_{6–8}$ methylbenzenes (benzene, toluene, *p*-xylene, *m*-xylene, *o*-xylene) in a MFI zeolite framework are correlated with their shortest molecular dimensions estimated using critical diameters [12–14] or kinetic diameters [15,16]. Kinetic (or collision) diameters (d_{kin}), derived from Lennard-Jones potentials, are molecular size descriptors that reflect the closest intermolecular distance for two identical spherical-shaped molecules colliding with zero intermolecular potential energy [15,16]. The critical diameter (d_{crit}) describes the diameter of the smallest cylinder that can circumscribe the lowest energy conformation of a molecule, and is related to the equilibrium diameter of a molecule at the minimum of the Lennard-Jones potential energy [12–15]. Although these static geometric descriptors capture some relevant size and shape features of species confined within microscopic voids, they do not account for the non-spherical shapes of bound species or the dynamic structural distortions of the zeolite host and organic guests [17–22]. Nevertheless, critical and kinetic diameters provide a means to qualitatively compare differences in intracrystalline diffusivities among various methylbenzenes in a given aluminosilicate topology, especially for the bulkier C_{9+} methylbenzenes which are unable to diffuse through MFI crystallites at reasonable experimental time scales. The reported critical diameters of all 13 methylbenzenes and the kinetic diameters of some methylbenzenes are summarized in Table S1.

Table S1. Molecular dimensions of methylbenzenes

Molecule	Critical diameter[a], d_{crit} / nm	Kinetic diameter[b], d_{kin} / nm
Benzene	0.66	0.585
Toluene	0.66	0.585
para-Xylene	0.66	0.585
ortho-Xylene	0.73	0.680
meta-Xylene	0.73	0.680
1,2,4-Trimethylbenzene	0.73	0.680
1,2,3-Trimethylbenzene	0.76	-
1,3,5-Trimethylbenzene	0.82	0.760
1,2,4,5-Tetramethylbenzene	0.74	-
1,2,3,4-Tetramethylbenzene	0.77	-
1,2,3,5-Tetramethylbenzene	0.82 × 0.89	-
Pentamethylbenzene	0.82 × 0.91	-
Hexamethylbenzene	0.91	-

[a] From references [12–14].
[b] From references [8,15,23].

Section S3. Additional discussion on DTBP cofeed experiments in MCM-41 and MFI zeolites

In this section, we provide further discussion on the induction behavior during toluene methylation with DME on MCM-41 (in the presence or absence of DTBP) and additional evidence that DTBP does not impact rates of deactivation of intracrystalline H^+ sites in MFI zeolites.

The MCM-41 sample is a meso-structured amorphous aluminosilicate that is known to have significant amounts of silanol and non-tetrahedral Al species [24,25]. Previous studies [26,27] have shown that DME (or methanol) is effective at healing connectivity defects in certain solid acids (e.g., SiO_2/Al_2O_3, ZrO_2) through hydrolysis or reforming reactions with hydroxyl groups (423–723 K). Such transformations of proximal silanol groups and Lewis acidic Al sites into Brønsted acid sites (often referred to as pseudo-bridging silanols [28,29]) most likely explain the induction transient in MCM-41 during toluene methylation with DME. The results from toluene methylation with DTBP co-feed (Fig. 4a, main text) confirm that Brønsted acid sites on MCM-41 solely catalyze toluene methylation reactions and that Lewis acid sites do not contribute to measured rates unless they first restructure into Brønsted acid sites.

During toluene methylation with DTBP co-feed on MCM-41, DTBP was fed in small concentrations (5 Pa) that are insufficient to titrate all of the H^+ sites within the MCM-41 packed-bed in less than 1 hour time-on-stream, as seen in the complete disappearance of DTBP in the reactor effluent (Fig. S5) [1]. These sub-stoichiometric DTBP co-feed amounts coupled with the induction transient in MCM-41, explain the 2 h delay in DTBP's ability to poison all Brønsted acid sites (both present initially and formed *in-situ*) on MCM-41. Furthermore, the DTBP uptake (0.10 ± 0.01 DTBP per Al_{total})) is 3× lower than that obtained using NH_4^+ titration (0.30 ± 0.03 NH_3 evolved per Al_{total}). On the other hand, unlike in the MCM-41 aluminosilicate, the MFI zeolites have much lower numbers of external H^+ sites and were exposed to higher DTBP concentrations (9–40 Pa) to completely eliminate all external H^+ sites in the MFI packed-beds at initial times-on-stream, as confirmed by the near-unity fraction of DTBP recovered in the reactor effluent during the first GC injection (~10 mins time on stream) (Fig. S6).

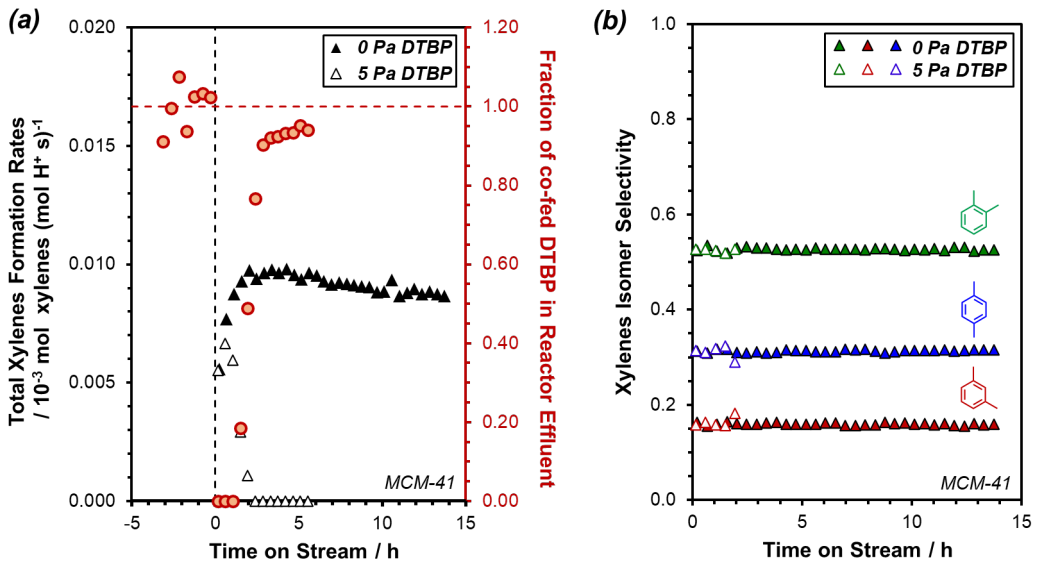

Figure S5 (a) Total xylenes formation rates alongside fractions of co-fed DTBP in reactor bypass or effluent, and (b) xylene isomer selectivity as a function of time-on-stream during toluene methylation (4.0 kPa toluene, 66 kPa DME, 403 K) with and without DTBP cofeed (5 Pa DTBP) on MCM-41. The red horizontal dashed line in (a) reflects the normalized average concentration of DTBP in reactor bypass stream before reaction. Reproduced with permission from Ezenwa et al. [1]. Copyright 2024 American Chemical Society.

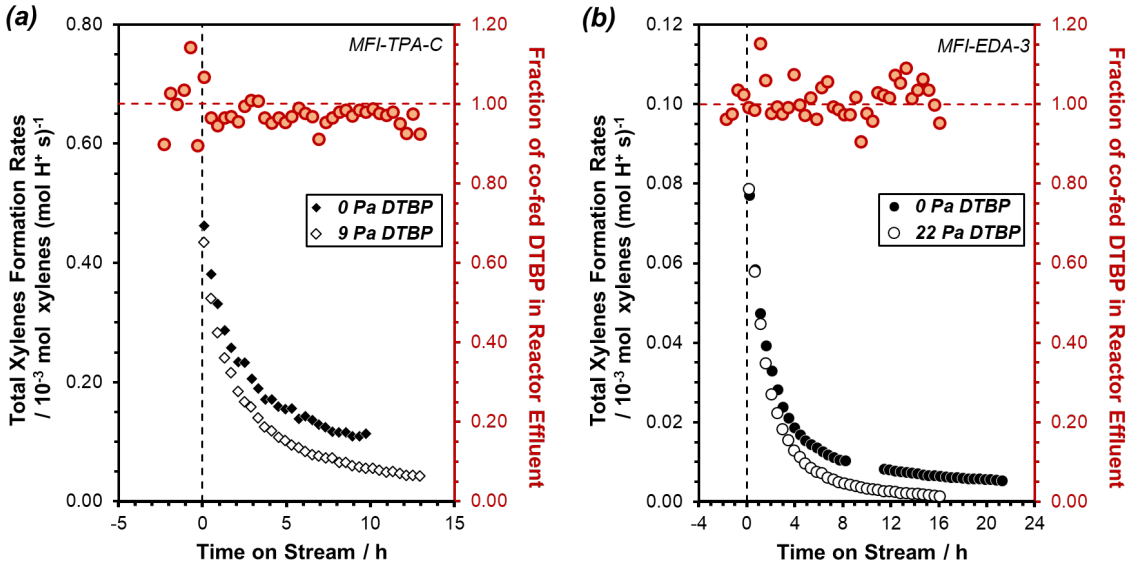

Figure S6. Total xylenes formation rates and fractions of co-fed DTBP in reactor bypass or effluent as a function of time-on-stream during toluene methylation (4.0–4.2 kPa toluene, 66 kPa DME, 403 K) with and without DTBP cofeeds on (a) MFI-TPA-C (9 Pa DTBP) and (b) MFI-EDA-3 (22 Pa DTBP). The red horizontal dashed lines reflect the normalized average concentration of DTBP in reactor bypass stream before reaction.

Furthermore, we have provided additional discussions and data to support our claim that DTBP does not cause additional transport restrictions or exacerbate the deactivation of intracrystalline H^+ sites in MFI zeolites during low-temperature toluene methylation. In our previous study [1], we showed that during toluene methylation with methanol (2 kPa toluene, 4 kPa MeOH, 403 K), the deactivation of MFI zeolites is negligible, partly because the reaction rates are much lower (~100×) due to the different identity and concentration of methylating agent in that experiment (4 kPa CH_3OH) compared to the current study (65 kPa DME). We showed that on two different MFI-TPA samples (MFI-TPA-C, Si/Al 43; MFI-TPA-C1, Si/Al 31), co-feeding DTBP (20–40 Pa) negligibly (<10%) alters rates and selectivity even after feeding 2.5 cumulative DTBP per Al_{total} (Fig S7–S8). However, upon introducing pyridine (20 Pa), rates are fully suppressed after 0.9 cumulative pyridine per Al_{total} have been fed. These results indicate that at our reaction temperature (403 K), DTBP is relegated to external surfaces and does not cause any pore blockage. Moreover, across all our studies on the MFI-TPA samples (with DME and MeOH), we do not observe increases in selectivity to the faster diffusing *p*-X isomer with DTBP co-feeds, which provides another indication that DTBP does not alter molecular transport rates between the intracrystalline regions and extracrystalline fluid phases.

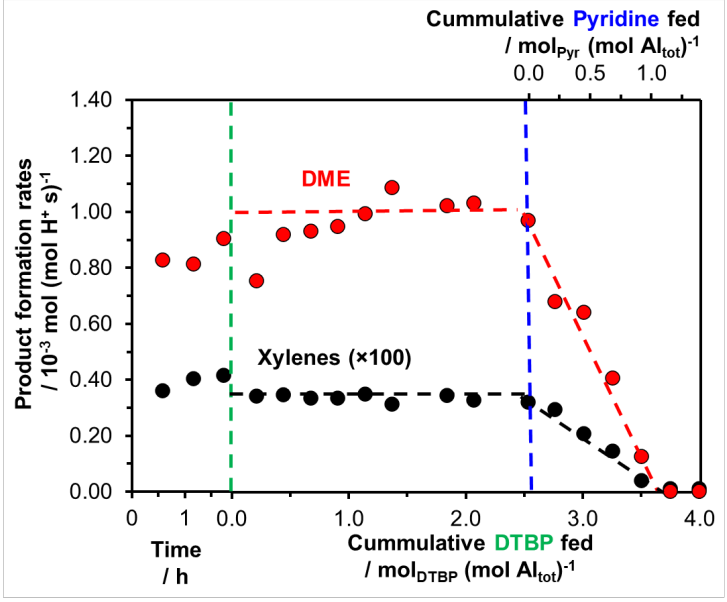

Figure S7. Xylenes and DME STY before and after titrant introduction (20 Pa DTBP and 20 Pa Pyridine) during toluene methylation on MFI-TPA-C at 2 kPa toluene, 4 kPa methanol 403 K. Reproduced with permission from Ezenwa et al. [1]. Copyright 2024 American Chemical Society.

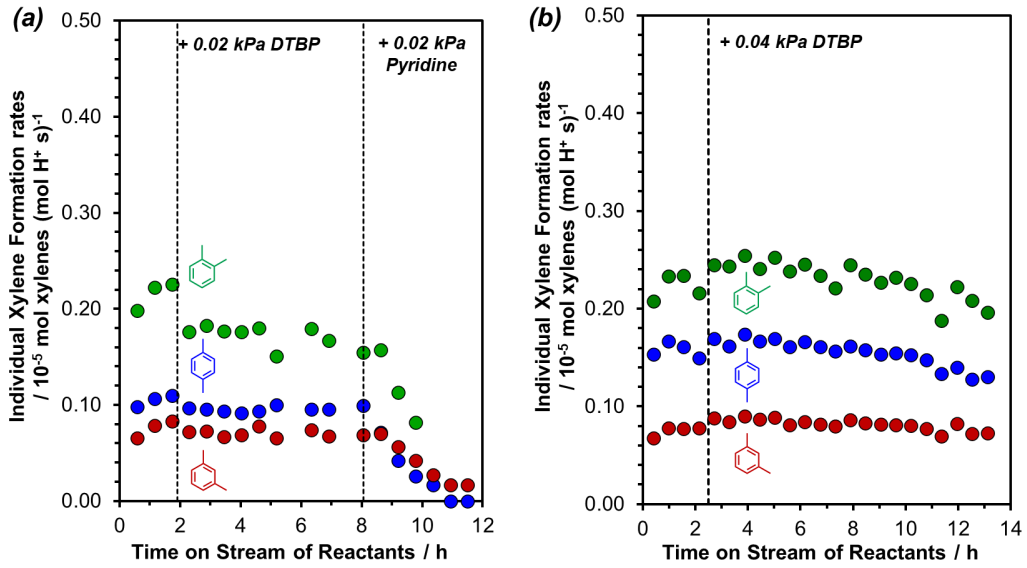

Figure S8. Individual xylenes formation rates vs time-on-stream during toluene methylation (2 kPa toluene, 4 kPa MeOH, 403 K) before and after titrant (20–40 Pa DTBP, 20 Pa Pyridine) introduction on **(a)** MFI-TPA-C (Si/Al 43) **(b)** MFI-TPA-C1 (Si/Al 31). Because of an overlap of the pyridine GC peak and *o*-X GC peak, the *o*-X formation rates could not be quantified past 10 h time-on-stream (0.7 moles Pyridine fed per Al) during pyridine cofeeds. Slight discontinuity during titrant introduction result from non-systematic experimental artefacts of swapping syringes with and without titrants. Reproduced with permission from Ezenwa et al. [1]. Copyright 2024 American Chemical Society.

We also compare the deactivation profiles of the unconfined MCM-41 with those of the extracrystalline H^+ sites of MFI zeolites, obtained by subtracting the deactivation profiles of MFI zeolites in the presence and absence of DTBP co-feeds (Fig. S9–S10 below). The results show that the slopes of the deactivation profiles of unconfined H^+ sites are essentially similar on both MFI zeolites and MCM-41 (Fig. S10). We also observe that the difference profile in MFI-TPA-C666 is almost twice (1.6×) that of the MFI-TPA-C (Fig. S10), which likely reflects the roughly twice (2.4×) larger fractions of H^+_{ext}/H^+_{total} in MFI-TPA-C666 compared to MFI-TPA-C [30]. The difference profiles are essentially invariant with time-on-stream, further indicating that DTBP does not cause intracrystalline deactivation to become faster with time-on-stream, which would have manifested as an increasing trend in the difference profile. Rather, DTBP simply eliminates all extracrystalline H^+ sites to reveal deactivation behavior of intracrystalline H^+ sites.

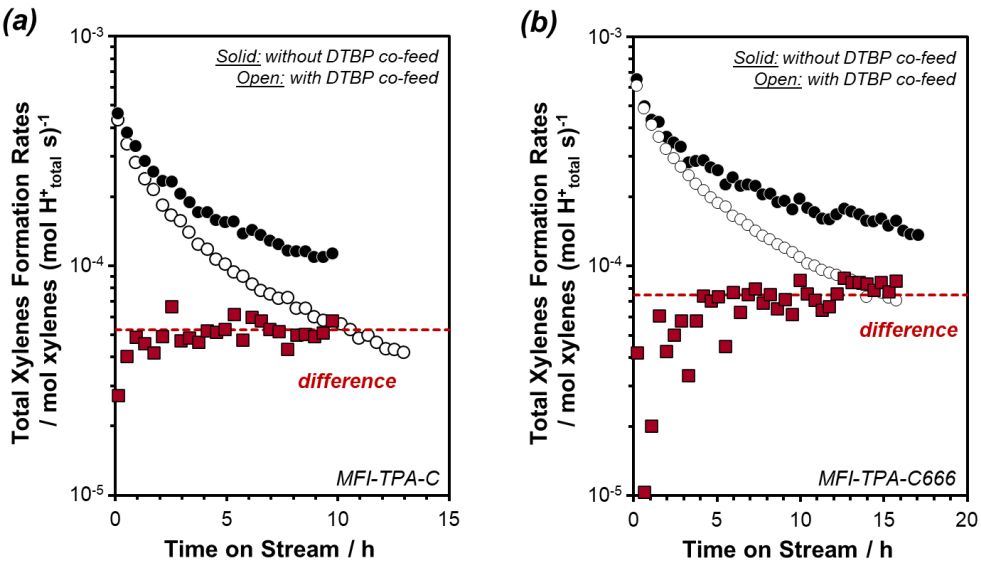

Figure S9. Differences in deactivation profiles during toluene methylation with DME in the presence and absence of DTBP on (a) MFI-TPA-C and (b) MFI-TPA-C666. The red horizontal dashed lines reflect the average of the rate differences after 5 h time on stream. Reaction conditions: 4.0 kPa Toluene, 66 kPa DME, 403K, <1% toluene conversion. For DTBP cofeed experiments, DTBP pressures are 0.008 kPa (MFI-TPA-C) and 0.015 kPa (MFI-TPA-C666). Uncertainties in rate measurements are 15% while uncertainties in rates differences are ~20%.

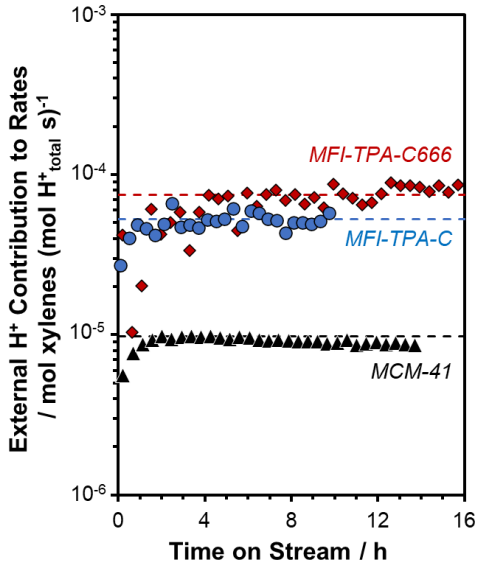

Figure S10. Comparison of differences in deactivation profiles during toluene methylation with DME in the presence and absence of DTBP on MFI-TPA-C and MFI-TPA-C666 with deactivation profile of MCM-41 in absence of DTBP cofeed. The red and blue horizontal dotted lines reflect the average of the rate differences after the 5 h time on stream. The black horizontal dashed lines reflect the maximum rate value on MCM-41. Reaction conditions: 4.0 kPa Toluene, 66 kPa DME, 403K, <1% toluene conversion.

The rates presented in Figures S9 and S10 are normalized by the total amount of H^+ sites quantified by NH_4^+ aqueous ion-exchange followed by NH_3 TPD. On MFI-TPA-C and MFI-TPA-C666 zeolites, the estimated reactivity of external sites (obtained from re-normalizing the difference profile in the presence and absence of DTBP by the external H^+ site counts obtained by DTBP [30]) are similar 6–10 $\times 10^{-4}$ mol xylenes (mol H^+_{ext} s)$^{-1}$. This range of values are, however, much higher than the rates on MCM-41 when normalized by either NH_3 (1.0×10^{-5} mol xylenes (mol H^+ s)$^{-1}$) or the DTBP uptake (3.5×10^{-5} mol xylenes (mol H^+ s)$^{-1}$). Although external H^+ sites on MFI zeolites are expected to be similar to unconfined H^+ sites on MCM-41, these results suggest that there might still be some kinetic differences between external H^+ sites on these two samples. We emphasize that rate comparisons across aluminosilicates are very sensitive to normalizations that assume all sites titrated *ex-situ* contribute equally to measured rates.

Section S4. Post-reaction studies on MFI using temperature programmed desorption

The total number of turnovers ($\mathrm{TON}_{effluent}$) to aromatics (i.e., methyl groups added to toluene per proton) observed in the effluent during toluene methylation at 403 K was estimated from the integrated formation rates of xylenes and 1,2,4-triMB during the reaction run (before reactant cutoff) normalized by the number of protons initially present in the reactor bed (Equation S1):

$$\mathrm{TON}_{effluent}(t_{rxn}) = \frac{\int_0^{t_{rxn}} dt \sum_j (n_{CH_3,j} - 1)\, F_{Xylene,j\ or\ 124TriMB}(t)}{H^+_{initial}} \qquad \text{(S1)}$$

The total number of turnovers to occluded polymethylbenzenes (TON_{PMB}; i.e., methyl groups added to toluene per proton) was estimated by subtracting the total number of aromatic rings (each ring originates from a toluene molecule containing one methyl substituent) from the total number of methyl groups in the hydrocarbons integrated over the time duration of the temperature ramp and normalized by the number of protons initially present in the reactor bed (Equation S2):

$$\mathrm{TON}_{PMB} = \frac{\int_{t_{initial,ramp}}^{t_{final,ramp}} dt \sum_j n_{CH_3,j} F_{j,hydrocarbon}(t) - \int_{t_{initial}}^{t_{final}} dt \sum_j F_{j,aromatic}(t)}{H^+_{initial}} \qquad \text{(S2)}$$

The calculated value of TON_{PMB} was found to be 5.2 mol CH_3-added (mol H^+)$^{-1}$.

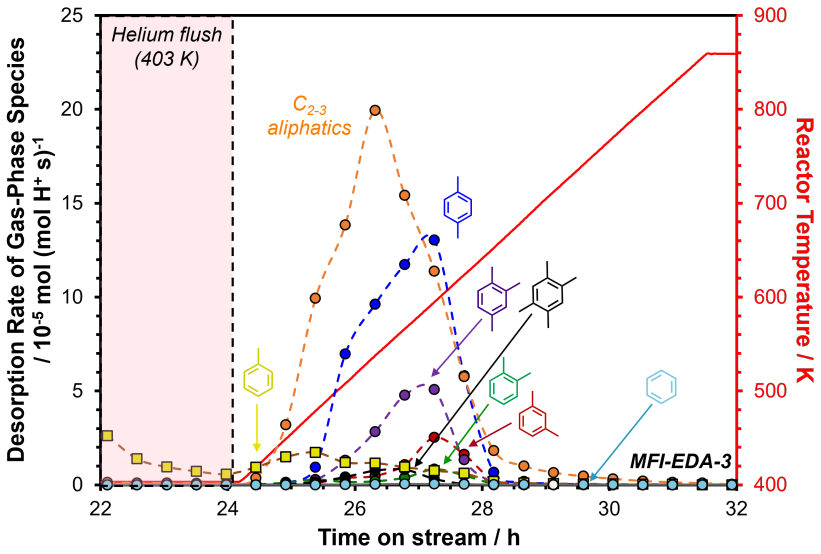

Figure S11. Desorption rates of gas-phase aliphatic and aromatic species during temperature ramp from 403 K to 853 K (0.033 K s^{-1}). Pink region represents a 2 h flush step after the 1st reaction run.

References

[1] S. Ezenwa, H. Montalvo-Castro, A.J. Hoffman, H. Locht, J. Attebery, D.-Y. Jan, M. Schmithorst, B. Chmelka, D. Hibbitts, R. Gounder, Synthetic Placement of Active Sites in MFI Zeolites for Selective Toluene Methylation to para-Xylene, J. Am. Chem. Soc. 146 (2024) 10666–10678. https://doi.org/10.1021/jacs.4c00373.

[2] B.L. Foley, B.A. Johnson, A. Bhan, A Method for Assessing Catalyst Deactivation: A Case Study on Methanol-to-Hydrocarbons Conversion, ACS Catal. (2019) 7065–7072. https://doi.org/10.1021/acscatal.9b01106.

[3] Z. Shi, A. Bhan, Metrics of performance relevant in methanol-to-hydrocarbons catalysis, J. Catal. 421 (2023) 198–209. https://doi.org/10.1016/j.jcat.2023.03.022.

[4] F.L. Bleken, T.V.W. Janssens, S. Svelle, U. Olsbye, Product yield in methanol conversion over ZSM-5 is predominantly independent of coke content, Microporous Mesoporous Mater. 164 (2012) 190–198. https://doi.org/10.1016/j.micromeso.2012.06.020.

[5] D. Chen, H.P. Rebo, K. Moljord, A. Holmen, Influence of Coke Deposition on Selectivity in Zeolite Catalysis, Ind. Eng. Chem. Res. 36 (1997) 3473–3479. https://doi.org/10.1021/ie9700223.

[6] J. Wei, A mathematical theory of enhanced para-xylene selectivity in molecular sieve catalysts, J. Catal. 76 (1982) 433–439. https://doi.org/10.1016/0021-9517(82)90272-X.

[7] G. Mirth, J. Cejka, J.A. Lercher, Transport and Isomerization of Xylenes over HZSM-5 Zeolites, J. Catal. 139 (1993) 24–33. https://doi.org/10.1006/jcat.1993.1003.

[8] C.D. Baertsch, H.H. Funke, J.L. Falconer, R.D. Noble, Permeation of Aromatic Hydrocarbon Vapors through Silicalite−Zeolite Membranes, J. Phys. Chem. 100 (1996) 7676–7679. https://doi.org/10.1021/jp960226h.

[9] S.J. Reitmeier, O.C. Gobin, A. Jentys, J.A. Lercher, Influence of Postsynthetic Surface Modification on Shape Selective Transport of Aromatic Molecules in HZSM-5, J. Phys. Chem. C 113 (2009) 15355–15363. https://doi.org/10.1021/jp905307b.

[10] O.C. Gobin, S.J. Reitmeier, A. Jentys, J.A. Lercher, Comparison of the Transport of Aromatic Compounds in Small and Large MFI Particles, J. Phys. Chem. C 113 (2009) 20435–20444. https://doi.org/10.1021/jp907444c.

[11] M. DeLuca, D. Hibbitts, Predicting diffusion barriers and diffusivities of C6–C12 methylbenzenes in MFI zeolites, Microporous Mesoporous Mater. 333 (2022) 111705. https://doi.org/10.1016/j.micromeso.2022.111705.

[12] V.R. Choudhary, V.S. Nayak, T.V. Choudhary, Single-Component Sorption/Diffusion of Cyclic Compounds from Their Bulk Liquid Phase in H-ZSM-5 Zeolite, Ind. Eng. Chem. Res. 36 (1997) 1812–1818. https://doi.org/10.1021/ie960411h.

[13] C.E. Webster, R.S. Drago, M.C. Zerner, Molecular Dimensions for Adsorptives, J. Am. Chem. Soc. 120 (1998) 5509–5516. https://doi.org/10.1021/ja973906m.

[14] C.E. Webster, R.S. Drago, M.C. Zerner, A Method for Characterizing Effective Pore Sizes of Catalysts, J. Phys. Chem. B 103 (1999) 1242–1249. https://doi.org/10.1021/jp984055n.

[15] D.W. Breck, Zeolite Molecular Sieves: Structure, Chemistry, and Use, Wiley, 1973.

[16] J.O. Hirschfelder, C.F. Curtiss, R.B. Bird, The Molecular Theory of Gases and Liquids, Revised edition, Wiley-Interscience, Hoboken, NJ, 1964.

[17] L.A. Clark, R.Q. Snurr, Adsorption isotherm sensitivity to small changes in zeolite structure, Chem. Phys. Lett. 308 (1999) 155–159. https://doi.org/10.1016/S0009-2614(99)00568-0.

[18] H. Xiong, Z. Liu, X. Chen, H. Wang, W. Qian, C. Zhang, A. Zheng, F. Wei, In situ imaging of the sorption-induced subcell topological flexibility of a rigid zeolite framework, Science 376 (2022) 491–496. https://doi.org/10.1126/science.abn7667.

[19] S. Wang, E. Iglesia, Catalytic diversity conferred by confinement of protons within porous aluminosilicates in Prins condensation reactions, J. Catal. 352 (2017) 415–435. https://doi.org/10.1016/j.jcat.2017.06.012.

[20] S. Herrmann, E. Iglesia, Elementary steps in acetone condensation reactions catalyzed by aluminosilicates with diverse void structures, J. Catal. 346 (2017) 134–153. https://doi.org/10.1016/j.jcat.2016.12.011.

[21] M.L. Sarazen, E. Iglesia, Effects of Charge, Size, and Shape of Transition States, Bound Intermediates, and Confining Voids in Reactions of Alkenes on Solid Acids, ChemCatChem 10 (2018) 4028–4037. https://doi.org/10.1002/cctc.201800401.

[22] S. Caro-Ortiz, E. Zuidema, M. Rigutto, D. Dubbeldam, T.J.H. Vlugt, Effects of Framework Flexibility on the Adsorption and Diffusion of Aromatics in MFI-Type Zeolites, J. Phys. Chem. C (2020). https://doi.org/10.1021/acs.jpcc.0c08054.

[23] S.J. Reitmeier, O.C. Gobin, A. Jentys, J.A. Lercher, Influence of Postsynthetic Surface Modification on Shape Selective Transport of Aromatic Molecules in HZSM-5, J. Phys. Chem. C 113 (2009) 15355–15363. https://doi.org/10.1021/jp905307b.

[24] H. Kosslick, G. Lischke, B. Parlitz, W. Storek, R. Fricke, Acidity and active sites of Al-MCM-41, Appl. Catal. Gen. 184 (1999) 49–60. https://doi.org/10.1016/S0926-860X(99)00078-2.

[25] A. Jentys, K. Kleestorfer, H. Vinek, Concentration of surface hydroxyl groups on MCM-41, Microporous Mesoporous Mater. 27 (1999) 321–328. https://doi.org/10.1016/S1387-1811(98)00265-0.

[26] N.R. Jaegers, V. Danghyan, J. Shangguan, C. Lizandara-Pueyo, P. Deshlahra, E. Iglesia, Heterolytic C–H Activation Routes in Catalytic Dehydrogenation of Light Alkanes on Lewis Acid–Base Pairs at ZrO2 Surfaces, J. Am. Chem. Soc. 146 (2024) 25710–25726. https://doi.org/10.1021/jacs.4c07766.

[27] M. Xu, J.H. Lunsford, D.W. Goodman, A. Bhattacharyya, Synthesis of dimethyl ether (DME) from methanol over solid-acid catalysts, Appl. Catal. Gen. 149 (1997) 289–301. https://doi.org/10.1016/S0926-860X(96)00275-X.

[28] K. Larmier, C. Chizallet, S. Maury, N. Cadran, J. Abboud, A.-F. Lamic-Humblot, E. Marceau, H. Lauron-Pernot, Isopropanol Dehydration on Amorphous Silica–Alumina: Synergy of Brønsted and Lewis Acidities at Pseudo-Bridging Silanols, Angew. Chem. Int. Ed. 56 (2017) 230–234. https://doi.org/10.1002/anie.201609494.

[29] C. Chizallet, P. Raybaud, Pseudo-Bridging Silanols as Versatile Brønsted Acid Sites of Amorphous Aluminosilicate Surfaces, Angew. Chem. Int. Ed. 48 (2009) 2891–2893. https://doi.org/10.1002/anie.200804580.

[30] S. Ezenwa, G. M. Hopping, E. D. Sauer, T. Scott, S. Mack, R. Gounder, Quantification of extracrystalline acid sites in MFI zeolites after post-synthetic passivation treatments using mesitylene benzylation kinetics, React. Chem. Eng. 9 (2024) 1096–1112. https://doi.org/10.1039/D3RE00589E.